A Density Functional Study on the Stereoselectivity of Styrene Polymerization with *ansa*-Metallocene Catalyst

Sung Hoon Yang, June Huh, Jae Shick Yang, and Won Ho Jo*

Hyperstructured Organic Materials Research Center and School of Materials Science and Engineering, Seoul National University, Seoul 151-742, Korea

Received February 2, 2004; Revised Manuscript Received April 19, 2004

ABSTRACT: The insertion mechanism of styrene polymerization with a Cp-based *ansa*-matallocene catalyst (Cp = η^5-C_5H_5) was investigated by the density functional theory (DFT). The metallocene catalyst adopted in this study, $Si(CH_3)_2Cp_2Ti(CH_3)_2$, is experimentally known as a highly syndiospecific catalyst for styrene polymerization. A cationic species, $SiH_2Cp_2Ti^+-CH_3$, is used as an activated form of the catalyst for modeling the initiation of styrene polymerization when one calculates the first insertion of a styrene monomer into the cationic species. Calculations for the second insertion of styrene monomer into the product of the first insertion were also performed. The results of the second insertion of styrene monomer suggest that the frontside insertion of the second styrene leads to a H_β-transfer reaction, while the backside insertion, which is favored over the frontside insertion, produces a highly syndiotactic product without the H_β-transfer reaction. This is in agreement with the experimental result. In the backside styrene insertion, the transition state is characterized by a β-agostic interaction than an α-agostic interaction because the α-agostic interaction has the repulsive interactions between catalytic ligands and substituents bonded to C_α of growing polymer chain. The stereoselectivity of the backside insertion is rationalized by the chain-end-control mechanism, and this mechanism also rationalizes higher insertion steps of styrene monomers.

I. Introduction

There have been substantial interests in homogeneous metallocene catalysts as an alternative to classical Ziegler−Natta heterogeneous catalysts.[1] These new compounds, metallocene catalysts, have several desirable properties such as high activity and an ability to produce high-molecular-weight polymers with a narrow molecular-weight distribution. Moreover, it is possible to control rigorously stereoselectivity by tailoring metallocene ligands.[2−5]

Many experimental investigations have been undertaken to understand the mechanism of metallocene-based polymerization.[6−9] Experiments have focused mainly on the effect of metallocene structure on the stereospecificity of polymer. However, the experimental works have been unsatisfactory to fully elucidate the insertion mechanism of metallocene-based polymerization due to limitation of instrumental facility in monitoring the reaction in a molecular level.

As supplementary methods, theoretical studies such as ab initio calculation,[10−20] semiempirical approachs,[21−27] and the density functional theory (DFT)[28−35] have been performed with much attention on the subject of metallocene-based polymerization. The methods have given us a basic insight into the real mechanism, which controls stereo- or regioselectivity of polymerization, and have also provided a guideline to design new catalyst for polymers having desired properties.

Up to date, however, most of these theoretical studies have concentrated on olefin polymerization. Consequently, very few of the theoretical studies have been carried out for elucidating the reaction mechanism of metallocene-catalyzed styrene polymerization, although the styrene polymerization has attracted much interest from industry in the past decade[36] since syndiotactic polystyrene was first synthesized in 1985.[37] The only theoretical study on the metallocene-based styrene polymerization, to our knowledge, is a density functional study by Cavallo and co-workers,[38,39] who investigated the mechanism of chain-end stereocontrol in syndiospecific polymerization of styrene with the catalytic model based on $CpTi^+CH(Ph)CH_3$ species (Cp = η^5-C_5H_5, Ph = phenyl ring). Although their work provides some meaningful information on the coordination behavior of styrene monomer to the catalytic site, the explanation for the insertion mechanism is still unsatisfactory due to simplification of their model used for the catalytic ligand and a growing polymer chain. Moreover, possible side reactions were not fully investigated since the directionality of styrene approach was not taken into account. In summary, the complete mechanism of syndiospecific styrene polymerization with metallocene catalyst has been still unraveled.

In this paper, we investigate the insertion mechanism for styrene monomer into a Cp-based *ansa*-metallocene catalyst in order to elucidate the origin of the stereoselectivity of metallocene-based styrene polymerization. Especially, we focus on how the chirality of growing polymer chain affects the directionality of styrene insertion in relation with the stereoselectivity.

This paper is organized as follows. The details of the computational method are presented in the next section. In section III, the results of DFT calculations are presented for the first insertion into the cationic catalyst, i.e., $SiH_2Cp_2Ti^+-CH_3$, which is defined as an initiation in this study. In section IV, the results for the second monomer insertion are presented, and the directionality of the styrene monomer insertion is discussed in detail by comparing the energy profile of the

* To whom correspondence should be addressed: e-mail whjpoly@plaza.snu.ac.kr; Tel +82-2-880-7192; Fax +82-2-885-1748.

10.1021/ma0497815 CCC: $27.50
Published on Web 06/29/2004

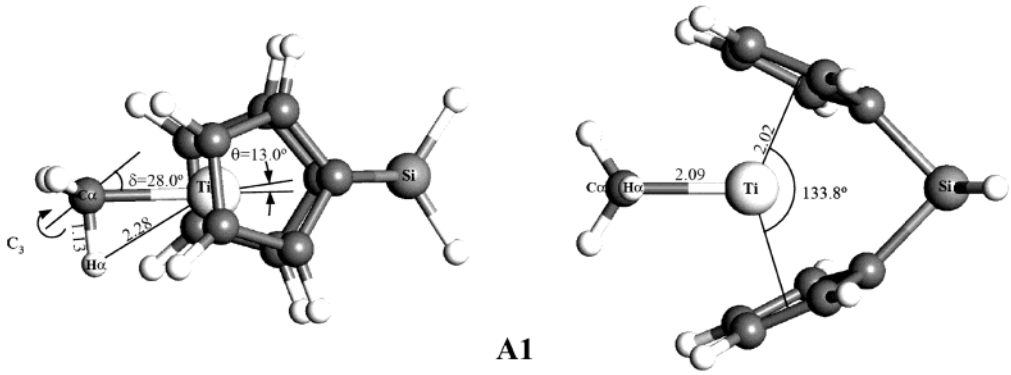

A1

Figure 1. Structure of cationic catalyst (**A1**), $SiH_2Cp_2Ti^+-CH_3$, for the first insertion of styrene, in which bond lengths and angles are in angstroms and degrees, respectively. The left picture is a top view and the right is a side view of **A1**.

frontside insertion with that of the backside insertion. Finally, we summarize our main results in the last section.

II. Computational Details

Fundamentals of the computational method are similar to our previous work.[40] All calculations were performed using the DMol^3 program (Accelrys Inc.) based on DFT.[41] Electronic configurations of molecular systems were described by restricted double-numerical basis sets with polarization functions for all atoms except for hydrogen. The $1s^22s^22p^6$ configuration on titanium was assigned to the core and treated by the frozen-core approximation. A geometry optimization was carried out using the Broydan−Fletcher−Goldfarb−Shanno[42−44] (BFGS) energy minimization algorithm for each molecule. The general gradient approximation (GGA) correction was applied to the energy calculation with the exchange functional of Becke[45] and the correlation functional of Perdew and Wang[46,47] after the energy was first calculated at the local density approximation (LDA) level.

The cationic methyl titanocene, $SiH_2Cp_2Ti^+-CH_3$, is used as a model catalyst to simplify the activated catalytic species of $Si(CH_3)_2Cp_2Ti(CH_3)_2$, which is a well-known *ansa*-metallocene catalyst for highly syndiospecific styrene polymerization.[48] The simplification of $Si(CH_3)_2$ by SiH_2 in the model catalyst is assumed to have a negligible effect on the reaction mechanism, although the electronic charge density on the Si atom might be slightly changed. The insertion of a styrene monomer was performed by a stepwise decrease in the reaction coordinate, followed by optimization of geometry with respect to all other degrees of freedom at each step. The reaction coordinate is defined as the distance between the C_α atom (i.e., the carbon which is directly attached to the titanium) and the carbon atom which is the nearest to C_α among carbon atoms of inserting monomer. For the H_β-transfer reaction, the reaction coordinate is defined as the distance between C_2 atom of monomer and H_β atom. The decrease in the reaction coordinate corresponds to an approach of a monomer toward the reactive site of the catalyst. By this stepwise insertion process described above, the reaction undergoes three distinctive states: π-complex, transition state, and product. The π-complex is a local minimum on the energy profile during monomer insertion, the transition state is a maximum point on the energy profile in the reaction coordinate between complex and product, and the product is an energetically global minimum point. This procedure was applied to all of monomer insertion processes.

Counterion effects were not taken into account in this study because it is too time-consuming to calculate the counterion effect in styrene insertion. However, some discussion on the counterion effect is given in the final section after a detailed description for the insertion mechanism.

III. Initiation

The optimized structure of the cationic methyl titanocene (**A1**) is shown in Figure 1. One of the interesting features in Figure 1 is that the structure exhibits an α-agostic interaction, which is obvious from a short $Ti-H_\alpha$ distance (2.28 Å), a large methyl tilt angle (δ = 28.0°), and an elongated $C_\alpha-H_\alpha$ bond length (1.13 Å) compared to the normal C−H bond length (1.10 Å). The electron deficiency of titanium induces the α-agostic interaction, which contributes to stabilizing the cationic catalyst. The strength of the agostic interaction is approximately estimated by performing single-point energy calculation at δ = 0° and by comparing the energy with that of corresponding fully optimized structure. The analysis reveals that the agostic interaction in the cationic titanocene stabilizes the structure by ca. 4 kcal/mol.

The Ti−Cen distance (where Cen denotes the center of Cp, 2.02 Å), the $Ti-C_\alpha$ bond length (2.09 Å), and the Cen−Ti−Cen angle (133.8°) are comparable to the experimental results for the nonbridged titanocene (2.072 Å, 2.162 Å, and 131.4°, respectively)[49] and also comparable to the results obtained by the ab initio molecular orbital method (2.084 Å, 2.049 Å, and 128.2°, respectively).[28]

The energy profile with the structure at each of stationary points for insertion of the first styrene is shown in Figure 2. The profile is calculated according to the Cossée−Arlman mechanism,[50] which is the most accepted reaction mechanism for the monomer insertion process. Furthermore, we assume that the insertion process of styrene monomer follows secondary (2,1-) insertion because the secondary insertion is experimentally known as the favored process for the styrene polymerization with this *ansa*-metallocene catalyst.[48] The overall behavior of the energy profile for styrene insertion is similar to that generally known for olefin insertion: (i) the π-complex is formed through an exothermic process (−19.42 kcal/mol) from isolated free reactants (i.e., the cationic catalyst (**A1**) and a styrene monomer), (ii) an energy barrier (ΔE = 9.30 kcal/mol)

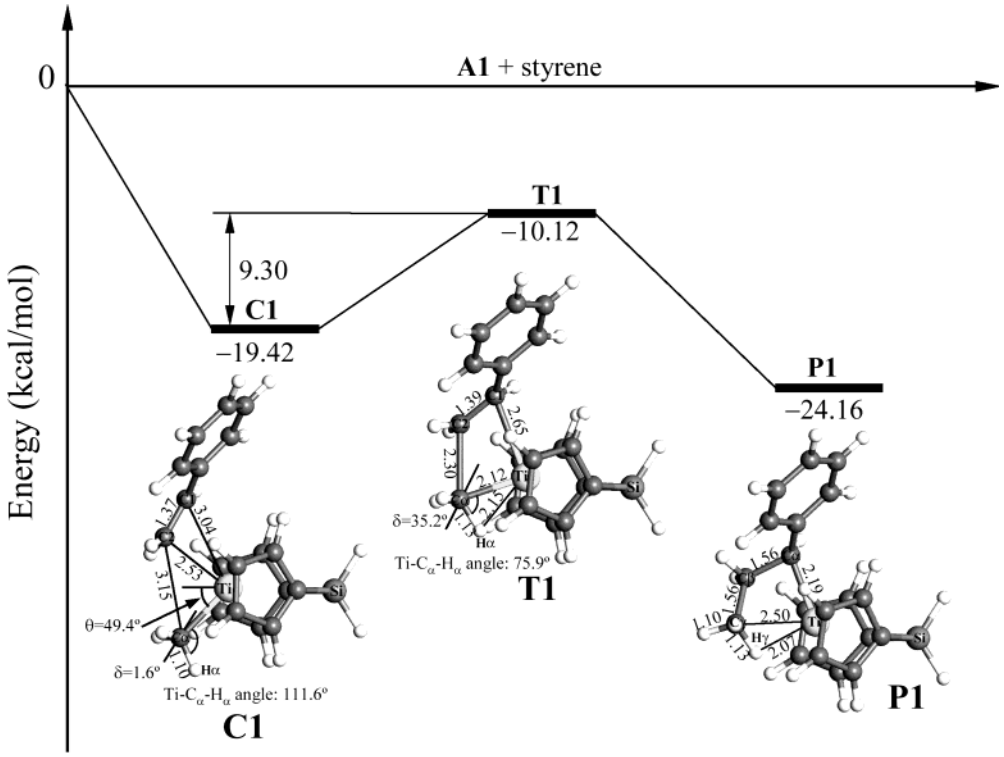

Figure 2. Energy profile and structures of π-complex (**C1**), transition state (**T1**), and product (**P1**) for the first insertion of styrene monomer; bond lengths in angstroms and angles in degrees. Energies are relative to the energy of isolated free reactants (**A1** + styrene monomer). Here the number 1 in the notations denotes the first insertion.

should be overcome for progressing to the final product, and (iii) the final product is energetically stabilized (−24.16 kcal/mol).

When the structure of the π-complex (**C1**) shown in Figure 2 is compared with the structure of cationic catalyst (**A1**) in Figure 1, it is realized that the molecular structure of the π-complex has some characteristic feature. First, as a styrene monomer approaches the cationic catalyst, the bent-sandwich angle (θ), i.e., the angle between the Ti−C_α bond vector and Cen−Ti−Cen plane, increases considerably from 13.0° to 49.4° in order to accommodate the approaching styrene monomer, which is consistent with previous reports that the bending motion of methyl group is very flexible.[51,52] Second, the methyl tilt angle (δ) decreases from 28.0° to 1.6°, and the C_α−H_α bond length is shortened from 1.13 to 1.10 Å, indicating that an α-agostic interaction is reduced by coupling of the electron-rich monomer and the cationic catalyst. It is also noteworthy that the distance of the Ti−C_1 (3.04 Å) is much longer than that of Ti−C_2 (2.53 Å); i.e., the complex is asymmetric, mainly due to unfavorable steric interaction between the phenyl ring of styrene monomer and the Cp rings of the catalyst.

At the transition state (**T1**), methyl tilt angle (δ) increases again from 1.6° to 35.2° to induce an α-agostic interaction which is obvious from both an elongated C_α−H_α length (from 1.10 to 1.13 Å) and a decreased Ti−C_α−H_α angle (from 111.6° to 75.9°) compared to those in the π-complex. The induced α-agostic interaction contributes to stabilizing the structure at the transition state, whereas the typical four-centered ring of Ti−C_1−C_2−C_α destabilizes the structure.

The product (**P1**), directly obtained from the transition state (**T1**) by enchainment of the first styrene monomer, shows a typical characteristic of γ-agostic structure, which is realized by a short H_γ−Ti distance (2.07 Å) and an elongated C_γ−H_γ bond length (1.13 Å) compared to the normal C−H bond length.

IV. Stereoselectivity

There are two pathways in the second insertion: the frontside vs the backside insertion of styrene monomer into the cationic catalyst. The frontside insertion is defined as the successive insertion of monomers at alternating side of the active catalyst, while the backside one is the insertion of every monomer at the same side of the active catalyst on polymerization. In this section, the structural characteristics and the energy profile for the frontside insertion and the backside insertion are discussed.

Frontside Insertion. Figure 3 represents a molecular structure of the catalyst (**A2$_f$**) for the second insertion of a styrene monomer, which is obtained from **P1** by rotating the $C_\beta H_2 C_\gamma H_3$ group around the C_α−C_β bond followed by energy minimization. The energy of **A2$_f$** (−31.03 kcal/mol) is lower than that of **P1** (−24.16 kcal/mol) by 6.87 kcal/mol, which is due to a strong β-agostic interaction in **A2$_f$** as shown by a highly elongated C_β−H_β bond length (1.17 Å).

The structure of **A2$_f$** is appropriate for the frontside insertion of a styrene because the reactive vacant site (represented by a block arrow in Figure 3) is open toward the opposite side to the approach direction of the first styrene, which is represented by a large bent-sandwich angle ($\theta = 32.2°$). The side view of the catalyst in Figure 3 shows relative positions of the phenyl ring of the inserted styrene and the Cp rings of the catalyst.

There are two possible modes in the second insertion of styrene via the frontside attack: one yields a meso diad of inserted styrene, which results in isotactic polystyrene, and the other yields a racemic diad, result-

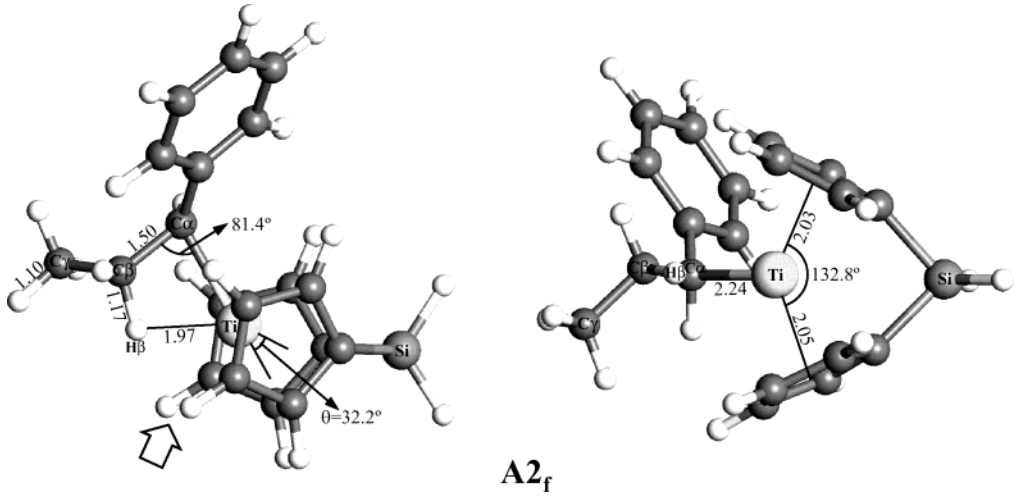

Figure 3. Structure of cationic catalyst, $SiH_2Cp_2Ti^+-CH(C_6H_5)CH_2CH_3$, for the frontside insertion (**A2f**); bond lengths in angstroms and angles in degrees. The left picture is a top view, and the right is a side view of **A2f**.

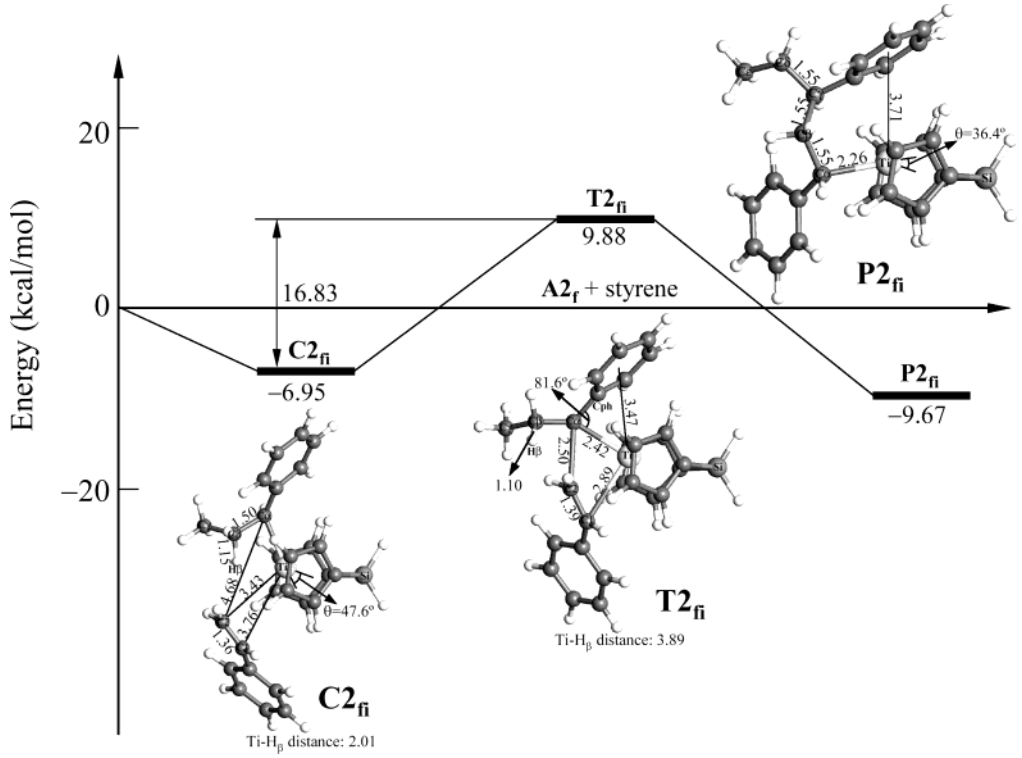

Figure 4. Energy profile and structures of π-complex (**C2fi**), transition state (**T2fi**), and product (**P2fi**) during chain propagation for the second insertion of styrene monomer via the frontside isotactic insertion; bond lengths in angstroms and angles in degrees. Energies are relative to the energy of isolated free reactants (**A2f** + styrene monomer). Here the number 2 and subscript fi in the notations denote the second and frontside isotactic insertion, respectively.

ing in syndiotactic polystyrene. The energy profiles and the structures of stationary points during the second styrene insertion are shown in Figures 4 and 5 for the isotactic and the syndiotactic insertions, respectively. The side view of the π-complex of the second styrene insertion is provided in the Supporting Information for visualization of tacticity of the second styrene insertion.

Some geometrical features of the π-complex of the second insertion (**C2fi** and **C2fs** for the isotactic and syndiotactic insertions, respectively) are similar to those of the first insertion process: (i) an increased bent-sandwich angle, θ (from 32.2° to 47.6° and 48.4° for **C2fi** and **C2fs**, respectively); (ii) asymmetric π-complexation (3.76 Å ($Ti-C_1$) and 3.43 Å ($Ti-C_2$) for **C2fi** and 3.70 Å ($Ti-C_1$) and 3.33 Å ($Ti-C_2$) for **C2fs**); (iii) the reduction of agostic interaction (reduced $C_\beta-H_\beta$ bond length from 1.17 to 1.15 Å for both **C2fi** and **C2fs**) compared to the cationic catalyst (**A2f** in Figure 3). However, the β-agostic interaction still remains strongly in the π-complex for the second insertion: the $C_\beta-H_\beta$ bond length of 1.15 Å in both **C2fi** and **C2fs** is still significantly longer than the normal C−H bond length of 1.10 Å. Consequently, the magnitude of exothermic energy gain in the π-complex for the second insertion (−6.95 and −6.82 kcal/mol for isotactic and syndiotactic insertions, respectively) is smaller than that for the first insertion (−19.42 kcal/mol shown in Figure 2).

The strong β-agostic interaction is broken at the transition state, which is shown by a considerably increased $Ti-H_\beta$ distance (3.89 Å for **T2fi** and 3.75 Å

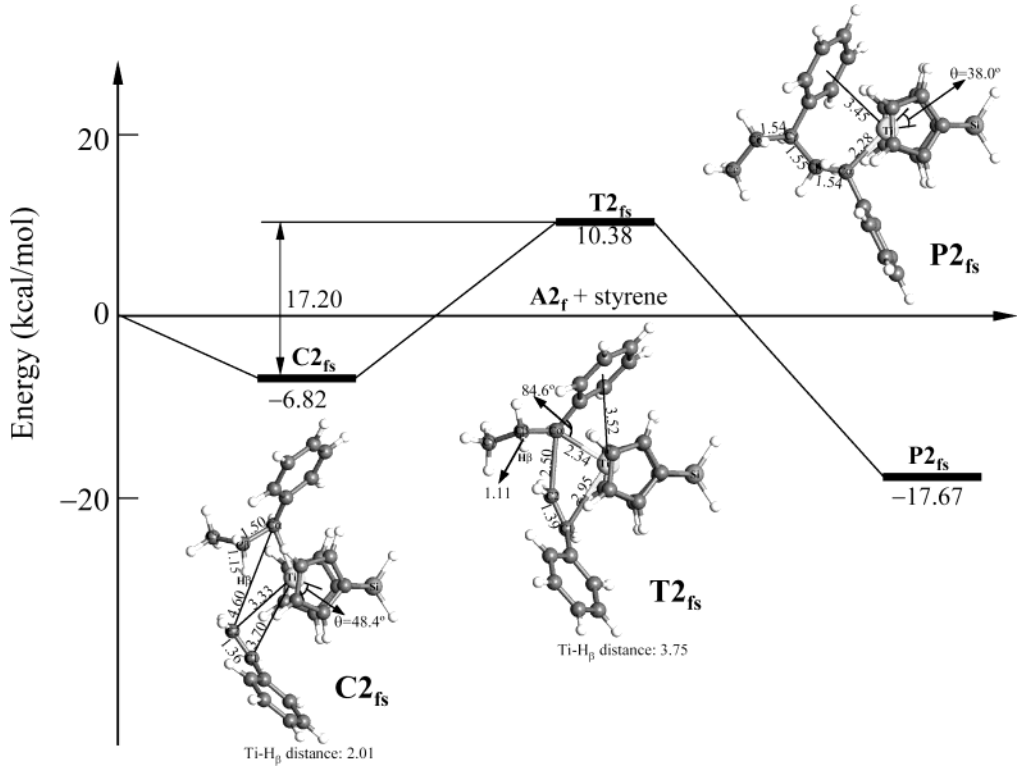

Figure 5. Energy profile and structures of π-complex (**C2$_{fs}$**), transition state (**T2$_{fs}$**), and product (**P2$_{fs}$**) during chain propagation for the second insertion of styrene monomer via the frontside syndiotactic insertion; bond lengths in angstroms and angles in degrees. Energies are relative to the energy of isolated free reactants (**A2$_f$** + styrene monomer). Here the number 2 and subscript fs in the notations denote the second and the frontside syndiotactic insertion, respectively.

for **T2$_{fs}$**) and almost completely recovered $C_\beta-H_\beta$ bond length (1.10 Å for **T2$_{fi}$** and 1.11 Å for **T2$_{fs}$**). Breakage of the β-agostic interaction and formation of a four-centered ring structure destabilizes the transition structures, **T2$_{fi}$** and **T2$_{fs}$**. As a result, the energy barrier for insertion of the second styrene becomes higher (16.83 and 17.20 kcal/mol for the isotactic and the syndiotactic insertions, respectively) as compared to that for the first insertion (9.30 kcal/mol). It should be pointed out that the difference in the energy barrier between the frontside isotactic and the frontside syndiotactic insertions is too small (0.37 kcal/mol) to rationalize the stereoselectivity of styrene polymerization with this *ansa*-metallocene catalyst, considering that the catalyst is experimentally known as a highly syndiospecific catalyst.[48]

Furthermore, the β-agostic interaction present in the π-complex for the frontside insertion can lead to another important reaction, i.e., the H_β-transfer reaction, instead of chain propagation, because the H_β atom is located in front of open active site due to the β-agostic interaction between H_β and titanium. Figures 6 and 7 show the energy profiles and the structures at stationary points for the H_β-transfer reaction. The reaction passes through three stationary points: (i) π-complex (**C2**), (ii) transition state (**T**β), and (iii) product (**C**β). The π-complex (**C2**) is exactly identical to that for chain propagation. At the transition state (**T**β), H_β plays a very critical role of stabilizing the structure by formation of a β-agostic interaction, which results in forming a double four-centered ring, as shown in **Tβ_{fi}** and **Tβ_{fs}**. The energy barrier for the H_β-transfer reaction is 14.44 kcal/mol for isotactic and 13.83 kcal/mol for syndiotactic insertion, which is lower than that for propagation (16.83 and 17.20 kcal/mol, respectively). This is because the β-agostic interaction for the H_β-transfer reaction stabilizes the transition structure **Tβ_{fi}** and **Tβ_{fs}**, whereas the β-agostic interaction is broken in **T2$_{fi}$** and **T2$_{fs}$** during chain propagation. Consequently, it is concluded that the frontside insertion of styrene monomer leads to a kinetically favorable H_β-transfer reaction rather than chain propagation. In summary, the frontside insertion of styrene monomer is not a plausible mechanism for styrene polymerization with the *ansa*-metallocene catalyst.

The product of the H_β-transfer reaction becomes another π-complex (**C**β), which is composed of a cationic catalyst having a styrene unit and a polymer chain terminated with a C═C double bond. A reverse reaction between the newly formed cationic catalyst and the C═C double bond at the end of the polymer chain is also possible, recovering the initial π-complex (**C2**). Other types of H_β-transfer reaction, i.e., the transfer to a metal center or to a counterion, are not taken into account in this study because we are concerned only about the H_β-transfer reaction as a side reaction of chain propagation.

Backside Insertion. The backside insertion, i.e., the insertion of every monomer at the same side of the active catalyst, is always accompanied by chain back-skip. Here, the chain back-skip involves rearrangement of the vacant site of the active catalyst, forming another conformational structure of the active catalyst. More specifically, the chain back-skip is described as an inversion of the $Ti-C_\alpha$ bond vector with respect to the Cen−Ti−Cen plane of **A2$_f$**. The mechanism of the chain back-skip can be regarded as a bending motion of the $Ti-C_\alpha$ bond vector, i.e., a decrease of the bent-sandwich angle, θ, without rotation of the growing polymer chain around the $Ti-C_\alpha$ bond axis, because the bulky phenyl

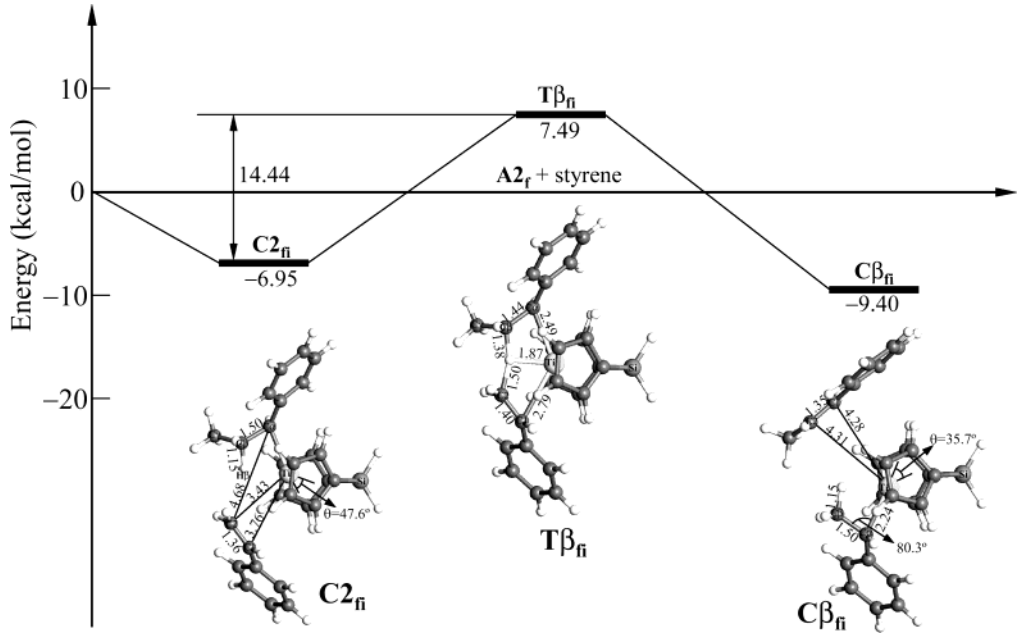

Figure 6. Energy profile and structures of π-complex (**C2$_{fi}$**), transition state (**Tβ_{fi}**), and product (**Cβ_{fi}**) during H_β-transfer reaction for the second insertion of styrene monomer via the frontside isotactic insertion; bond lengths in angstroms and angles in degrees. Energies are relative to the energy of isolated free reactants (**A2$_f$** + styrene monomer). Here the letter β and subscript fi in the notations denote the H_β-transfer reaction and the frontside isotactic insertion, respectively.

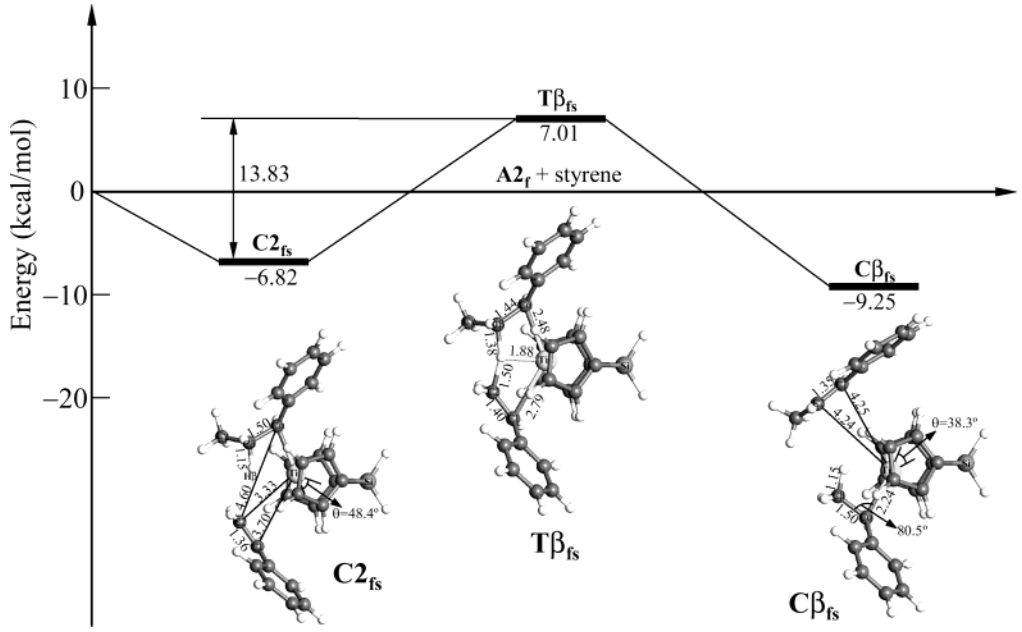

Figure 7. Energy profile and structures of π-complex (**C2$_{fs}$**), transition state (**Tβ_{fs}**), and product (**Cβ_{fs}**) during H_β-transfer reaction for the second insertion of styrene monomer via the frontside syndiotactic insertion; bond lengths in angstroms and angles in degrees. Energies are relative to the energy of isolated free reactants (**A2$_f$** + styrene monomer). Here the letter β and subscript fs in the notations denote the H_β-transfer reaction and the frontside syndiotactic insertion, respectively.

ring of the first inserted styrene prevents the growing chain from rotation.

Following the bending, the bending energy is plotted against the bent-sandwich angle (θ) in Figure 8. As shown in Figure 8, the activation energy for the chain back-skip is negligibly small, and **A2$_b$** is thermodynamically more stable than **A2$_f$** by 3.15 kcal/mol, which suggests that the chain back-skip is a kinetically fast and thermodynamically favorable process. In other words, the product of the first insertion is expected to take a form of **A2$_b$** appropriate for the backside insertion rather than that of **A2$_f$** for the frontside insertion. When the side view of **A2$_f$** in Figure 3 is compared with that of **A2$_b$** in Figure 9, it is realized that the repulsive interaction between the bulky phenyl ring of styrene and the ligands of catalyst in **A2$_b$** is reduced by the chain back-skip as compared to **A2$_f$**.

As shown in Figure 9, **A2$_b$** also shows a β-agostic interaction stabilizing the cationic catalyst, as manifested by short Ti−H_β distance (1.88 Å), small Ti−C_α−C_β angle (82.0°), and highly elongated C_β−H_β bond length (1.22 Å). An inversion of the bent-sandwich angle, θ, from 32.2° (in **A2$_f$**) to −10.0° (in **A2$_b$**) implies that **A2$_b$** is appropriate for the backside insertion of styrene represented by a block arrow.

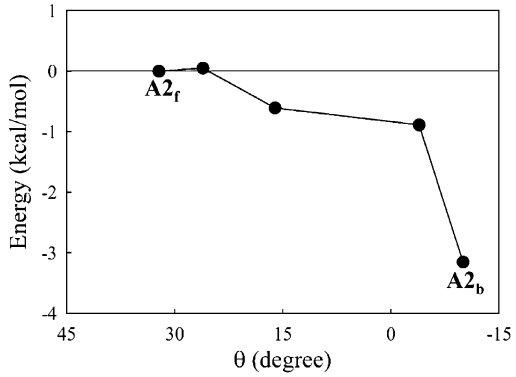

Figure 8. Calculated energy profiles for the chain back-skip from $\mathbf{A2_f}$ to $\mathbf{A2_b}$. The energy with change of the bent-sandwich angle, θ, is relative to the energy of $\mathbf{A2_f}$.

The energy profiles for the backside insertion of the second styrene monomer are shown with structures at each state in Figures 10 and 11 for the isotactic and the syndiotactic insertion, respectively. Here, the energy is relative to the sum of energies of a styrene monomer and the cationic catalyst, $\mathbf{A2_f}$. When the energy profile for isotactic insertion (Figure 10) is compared with that for syndiotactic insertion (Figure 11), it reveals that the energy barrier for enchainment of the second styrene monomer in the syndiotactic insertion (15.20 kcal/mol) is considerably lower than that of the isotactic insertion (18.22 kcal/mol), which indicates that the backside insertion rationalizes the syndiospecific stereoselectivity of the *ansa*-metallocene catalyst used in this study. A basic reason for this stereoselectivity of the catalyst is a repulsive interaction between two phenyl rings in two styrene units, i.e., the preinserted styrene and the second approaching one. Other views (Figure 12) of the transition structures for the isotactic ($\mathbf{T2_{bi}}$) and the syndiotactic insertion ($\mathbf{T2_{bs}}$) show more clearly that the isotactic insertion undergoes sterically more crowded state than does the syndiotactic insertion: in the isotactic insertion ($\mathbf{T2_{bi}}$), two phenyl rings of styrene monomers are located at the same side with respect to the plane defined by the C_1-C_2 bond vector and the

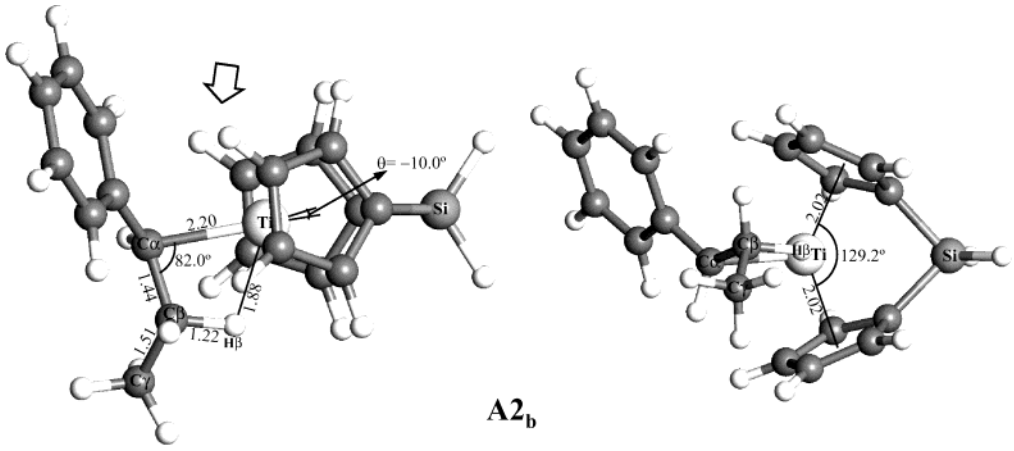

Figure 9. Structure of cationic catalyst, $SiH_2Cp_2Ti^+-CH(C_6H_5)CH_2CH_3$, for the backside insertion ($\mathbf{A2_b}$); bond lengths in angstroms and and angles in degrees. The left picture is a top view, and the right is a side view of $\mathbf{A2_b}$.

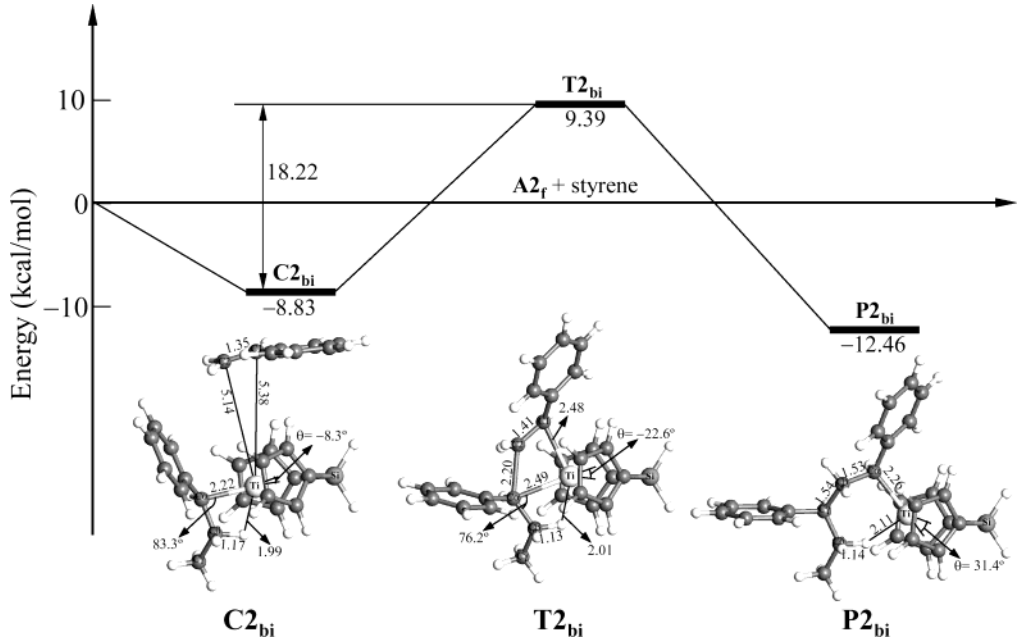

Figure 10. Energy profile and structures of complex ($\mathbf{C2_{bi}}$), transition state ($\mathbf{T2_{bi}}$), and product ($\mathbf{P2_{bi}}$) during chain propagation for the second insertion of styrene monomer via the backside isotactic insertion; bond lengths in angstroms and angles in degrees. Energies are relative to the energy of isolated free reactants ($\mathbf{A2_f}$ + styrene monomer). Here the number 2 and subscript bi in the notations denote the second insertion and the backside isotactic insertion, respectively.

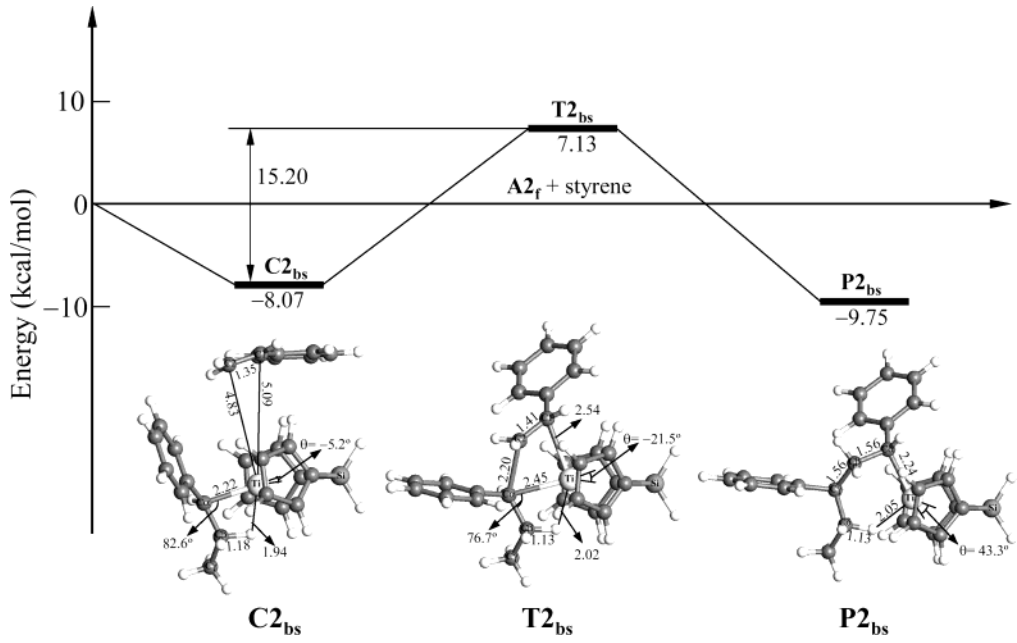

Figure 11. Energy profile and structures of complex (**C2$_{bs}$**), transition state (**T2$_{bs}$**), and product (**P2$_{bs}$**) during chain propagation for the second insertion of styrene monomer via the backside syndiotactic insertion; bond lengths in angstroms and angles in degrees. Energies are relative to the energy of isolated free reactants (**A2$_f$** + styrene monomer). Here, the number 2 and subscript bs in the notations denote the second insertion and the backside syndiotactic insertion, respectively.

titanium atom, while in the syndiotactic insertion (**T2$_{bs}$**), the two phenyl rings are separately located at different sides. Because the two phenyl rings and Cp ligands repulse each other, the more crowded transition state, **T2$_{bi}$**, has an essentially higher energy than **T2$_{bs}$**.

In general, a chiral site control,[53−55] which is assumed that the ligand controls directly the facial preference of an incoming monomer (*re*- or *si*-), has well explained the stereoselectivity of the catalysts based on stereorigid chiral metallocenes.[30,53,55,56] However, this cannot rationalize our results because the catalyst in our study is C_{2v}-symmetric, i.e., symmetrically achiral. In other words, this catalyst has inherently no preference between the isotactic and the syndiotactic insertion of styrene monomer. On the contrary, the chain-end-control mechanism, stating that the last inserted monomer controls the chirality of the next inserted monomer,[53,57,58] successfully explains the stereoselectivity in our case because the steric hindrance due to the phenyl ring of the preinserted styrene determines the energetics of insertion of the next styrene. Therefore, it is concluded that the chirality of insertion of the approaching styrene monomer, i.e., the stereoselectivity for the styrene insertion, is controlled by the chain-end-control mechanism.

It should be noted that the H_β-transfer reaction does not occur in the backside insertion because the H_β atom is *not* located in front of open active site while the second styrene monomer approaches the open active site accompanying with the chain back-skip. As a result, the β-agostic interaction is not broken by the insertion of styrene, and therefore the β-agostic interaction stabilizes the structure of transition state for the backside insertion. This β-agostic interaction is a very interesting feature because it has never been found in the case of olefin insertion, where an α-agostic interaction has been known as a major factor stabilizing the transition state.[59−61] Therefore, it is necessary to compare the energetics of the transition state showing a β-agostic interaction (**T2$_{bi}$** and **T2$_{bs}$**) with that showing an α-agostic interaction (**Tα$_{bi}$** and **Tα$_{bs}$**). The **Tα$_{bi}$** and **Tα$_{bs}$** were obtained from the **T2$_{bs}$** and **T2$_{bi}$**, respectively, by swapping the relative position of the ethyl group for the H atom bonded to C_α atom and by optimizing the energy of the structure in the presence of the identical constraint with **T2$_{bs}$** and **T2$_{bi}$** in their reaction coordinate. The result of energy calculation shows that, regardless of tacticity, the transition states showing an α-agostic interaction are energetically less stable (10.00 kcal/mol for **Tα$_{bi}$** and 9.32 kcal/mol for **Tα$_{bs}$**) than those showing a β-agostic interaction (9.39 kcal/mol for **T2$_{bi}$** and 7.13 kcal/mol for **T2$_{bs}$**). This is because the α-agostic structure has highly repulsive interactions between phenyl group of the preinserted styrene and Cp ring of catalyst ligands and between the ethyl group and the other Cp ring, as can be seen in Figure 13. The differences in insertion characteristics between olefin and styrene monomer can be rationalized by the difference in their regiospecificity: the olefin insertion proceeds via the primary insertion, i.e., no bulky group is bonded to C_α atom except the growing chain, whereas the styrene insertion proceeds via the secondary insertion resulting that two bulky groups, i.e., phenyl group and growing chain, are bonded to the C_α atom. Therefore, the transition state showing an α-agostic interaction is destabilized by the repulsive interaction between the bulky groups bonded to the C_α atom and catalytic ligands. In short, the styrene insertion into this type of metallocene catalyst follows the mechanism of syndiotactic backside insertion characterized by the β-agostic interaction at the transition state, where the energy barrier for enchainment of styrene is lower than any other enchainment processes of styrene.

Finally, the catalyst structure for the third insertion should be considered in order to generalize the insertion mechanism proposed for the second insertion, although the inserting process itself of the third styrene is not performed in this study. As described for the second insertion, the structure of catalyst for the backside insertion is thermodynamically more stable than that

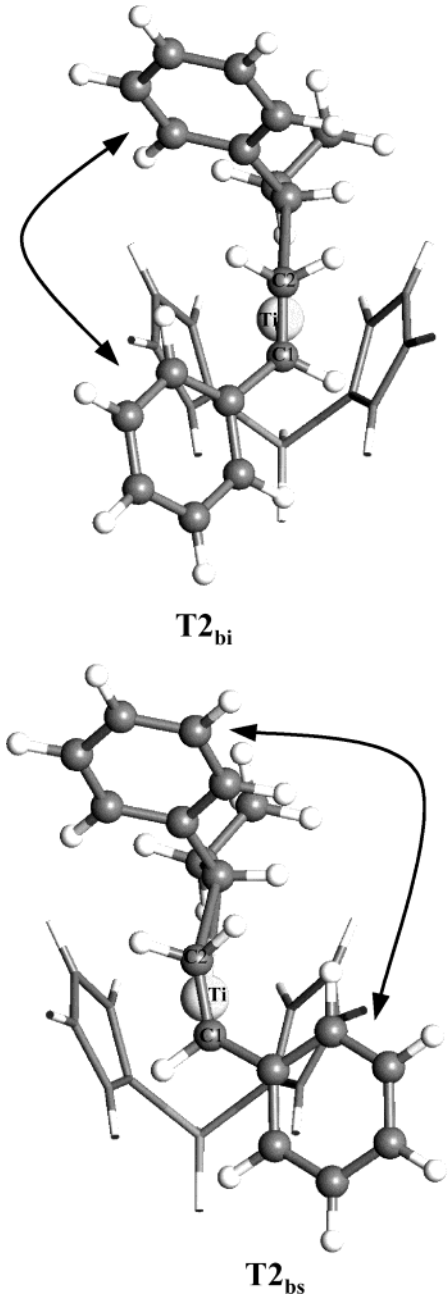

$\mathbf{T2_{bi}}$

$\mathbf{T2_{bs}}$

Figure 12. Side views of structures of transition states for the second backside isotactic ($\mathbf{T2_{bi}}$) and syndiotactic ($\mathbf{T2_{bs}}$) insertions. The arrows represent the interaction between two phenyl rings of the preinserted and the second approaching styrene monomers. The ligands of catalyst are represented by a thin stick mode for simplicity.

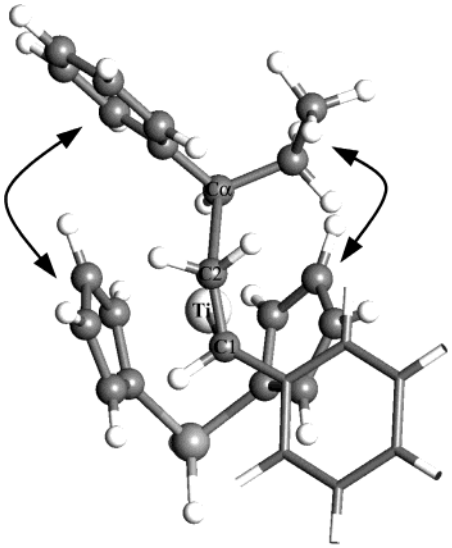

$\mathbf{T\alpha_{bi}}$

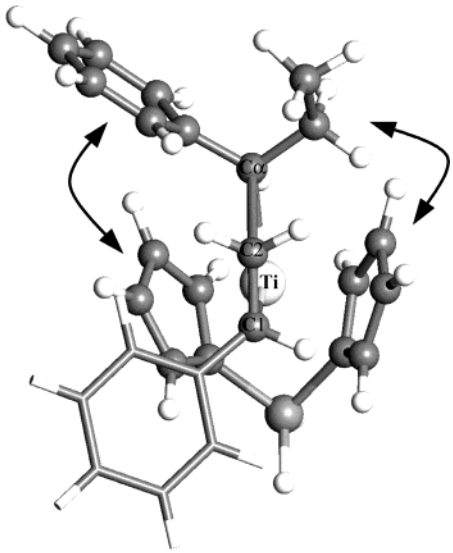

$\mathbf{T\alpha_{bs}}$

Figure 13. Structures of transition states for the isotactic ($\mathbf{T\alpha_{bi}}$) and the syndiotactic ($\mathbf{T\alpha_{bs}}$) insertions showing an α-agostic interaction. Two arrows of each structure represent the repulsive interactions between phenyl ring of the preinserted styrene and one of Cp ring of catalyst ligands and between the ethyl group and the other Cp ring. The phenyl ring of the second styrene monomer is represented by a thin stick mode for simplicity.

for the frontside insertion due to relief of the repulsive interaction between the phenyl ring of the preinserted styrene monomer and the ligand of the catalyst in the former case. This is the most important factor supporting the fact that the backside insertion is a dominant process, which yields highly syndiospecific polystyrene. To confirm that the mechanism proposed for the second insertion is also acceptable for the third insertion, two structures of the catalyst, i.e., one for frontside insertion ($\mathbf{A3_f}$ in Figure 14) and the other for backside insertion ($\mathbf{A3_b}$ in Figure 14), are first generated by changing the conformational structure of the syndiotactic product obtained via the backside insertion ($\mathbf{P2_{bs}}$) and then compared with each other. Both cases show a β-agostic interaction, as shown in Figure 14, where a block arrow indicates the reactive vacant site. Relative energies of the two structures are −21.51 kcal/mol for $\mathbf{A3_f}$ and −23.62 kcal/mol for $\mathbf{A3_b}$; i.e., the energy of $\mathbf{A3_b}$ is lower than that of $\mathbf{A3_f}$ by 2.11 kcal/mol, which is very consistent with the result for the second insertion. Similarly to the second insertion, it is also because the repulsive interaction in $\mathbf{A3_b}$ between the bulky phenyl ring of the last inserted (the second inserted in this study) styrene and the Cp ligands of the catalyst is lower than that in $\mathbf{A3_f}$. Therefore, it is concluded that the mechanism proposed for the second insertion can be expanded to higher insertions of styrene polymerization.

V. Summary

A DFT study on the origin of stereoselectivity for syndiotactic polymerization of styrene with *ansa*-met-

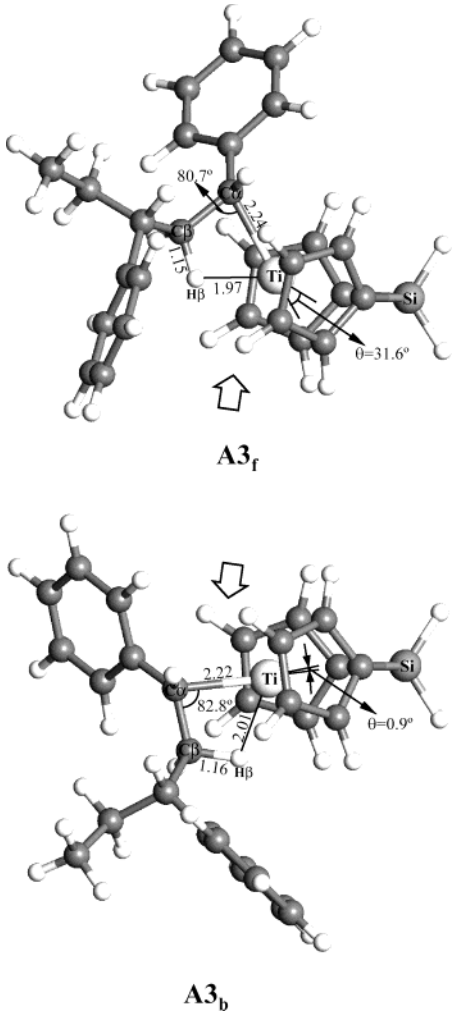

Figure 14. Structures of cationic catalyst, $SiH_2Cp_2Ti^+-(CH(C_6H_5)CH_2)_2CH_3$, for the third insertion. The top is for the frontside insertion (**$A3_f$**), and the other is for the backside insertion (**$A3_b$**); bond lengths in angstroms and and angles in degrees.

allocene is presented. It is found that the backside insertion is favored over the frontside insertion because the cationic catalyst for the backside insertion is thermodynamically more stable than that for the frontside insertion. The backside insertion mechanism explains the stereoselectivity of styrene insertion in accordance with the chain-end control, which is evident because the last inserted styrene monomer plays a critical role in determining the chirality of the next styrene monomer. The backside insertion mechanism can be summarized as follows: (i) the absence of the H_β-transfer reaction as a result of the chain back-skip and (ii) the propagation without breakage of the β-agostic interaction stabilizing the transition state, which results in reduction of the energy barrier for styrene insertion.

Although all explanations presented in this study satisfy self-consistency, an ambiguity still remains to be elucidated with regard to the role of counterion during styrene insertion. For example, in *real* catalytic system, the barrier to the back-skip might be increased due to the presence of a bulky counterion, and the counterion may also reduce the strength of agostic interaction stabilizing the transition state for monomer insertion by providing the cationic catalyst with electrons. The effect of the counterion on the monomer insertion during the metallocene-based polymerization has been the subject of our study and will be published in the future.

Acknowledgment. The authors thank the Korea Science and Engineering Foundation (KOSEF) through Hyperstructured Organic Materials Research Center (HOMRC) and Samsung General Chemicals Co. for their financial support.

Supporting Information Available: Side view of π-complex structure of the second styrene insertion, i.e., **$C2_{fi}$**, **$C2_{fs}$**, **$C2_{bi}$**, and **$C2_{bs}$**; optimized Cartesian coordinates and absolute energies of all stationary points. This material is available free of charge via the Internet at http://pubs.acs.org.

References and Notes

(1) Brintzinger, H. H.; Fischer, R.; Mülhaupt, R.; Rieger, B.; Waymouth, R. M. *Angew. Chem., Int. Ed. Engl.* **1995**, *34*, 1143.
(2) Kaminsky, W.; Külper, K.; Brintzinger, H. H.; Wild, F. R. W. P. *Angew. Chem.* **1985**, *97*, 507.
(3) Ewen, J. A.; Jones, R. L.; Razabi, A.; Ferrara, J. D. *J. Am. Chem. Soc.* **1988**, *110*, 6255.
(4) Natta, G.; Dnausso, F.; Sianesi, D. *Makromol. Chem.* **1958**, *28*, 253.
(5) Ishihara, N.; Seimiya, T.; Kuramono, M.; Uoi, M. *Polym. Prepr. Jpn.* **1986**, *35*, 240.
(6) Scheirs, J.; Kaminsky, W. *Metallocene-based Polyolefins: preparation, properties and technology*; John Wiley & Sons Ltd.: Chichester, 2000.
(7) Togni, A.; Halterman, R. L. *Metallocenes: Synthesis, Reactivity, Application*; Wiley-VCH: Weinheim, 1998.
(8) Long, N. J. *Metallocenes: An Introduction to Sandwich Complexes*; Blackwell Science: Malden, 1998.
(9) Tsvetkova, V. I. *Polym. Sci. Ser. C* **2000**, *42*, 2 and references reported therein.
(10) Novaro, O.; Blaisten-Barojas, E.; Clementi, E.; Giunchi, G.; Ruiz-Vizcaya, M. E. *J. Chem. Phys.* **1978**, *68*, 2337.
(11) Fuijimoto, H.; Yamasaki, T.; Mizutani, H.; Koga, N. *J. Am. Chem. Soc.* **1985**, *107*, 6157.
(12) Kawamura-Kuribayashi, H.; Koga, N.; Morakuma, K. *J. Am. Chem. Soc.* **1992**, *114*, 2359.
(13) Kawamura-Kuribayashi, H.; Koga, N.; Morokuma, K. *J. Am. Chem. Soc.* **1992**, *114*, 8687.
(14) Koga, N.; Yoshida, T.; Morokuma, K. *Organometallics* **1993**, *12*, 2777.
(15) Siegbahn, P. E. M. *Chem. Phys. Lett.* **1993**, *205*, 290.
(16) Weiss, H.; Ehrig, M.; Ahlrichs, R. *J. Am. Chem. Soc.* **1994**, *116*, 4919.
(17) Bierwagen, E. P.; Bercaw, J. E.; Goddard, W. A., III *J. Am. Chem. Soc.* **1994**, *116*, 1481.
(18) Doremaele, G. H. J.; Meier, R. J.; Iarlori, S.; Buda, F. *J. Mol. Struct.* (*THEOCHEM*) **1996**, *363*, 269.
(19) Linnolahti, M.; Pakkanen, T. A. *Macromolecules* **2000**, *33*, 9205 and references reported therein.
(20) Lanza, G.; Fragala, I. L.; Marks, T. J. *Organometallics* **2001**, *20*, 4006.
(21) Amstrong, D. R.; Pekins, P. G.; Stewart, J. J. P. *J. Chem. Soc., Dalton Trans.* **1972**, 9172.
(22) Cassoux, P.; Crasnifer, F.; Labarre, J.-F. *J. Organomet. Chem.* **1979**, *165*, 303.
(23) McKinney, R. J. *J. Chem. Soc., Chem. Commun.* **1980**, 490.
(24) Balazs, A. C.; Johnson, K. H. *J. Chem. Phys.* **1982**, *77*, 3148.
(25) Shiga, A.; Kawamura, H.; Ebara, T.; Sasaki, T. *J. Organomet. Chem.* **1989**, *266*, 95.
(26) Prosenc, M.-H.; Janiak, C.; Brintzinger, H.-H. *Organometallics* **1992**, *11*, 4036.
(27) Coussens, B. B.; Buda, F.; Oevering, H.; Meier, R. J. *Organometallics* **1998**, *17*, 795.
(28) Woo, T. K.; Fan, L.; Ziegler, T. *Organometallics* **1994**, *13*, 2252.
(29) Fan, L.; Harrison, D.; Deng, L.; Woo, T. K.; Swerhone, D.; Ziegler, T. *Can. J. Chem.* **1995**, *73*, 989.
(30) Lohrenz, J. C. W.; Woo, T. K.; Fan, L.; Ziegler, T. *J. Organomet. Chem.* **1995**, *497*, 91.
(31) Woo, T. K.; Margl, P. M.; Lohrenz, J. C. W.; Blöchl, P. E.; Ziegler, T. *J. Am. Chem. Soc.* **1996**, *118*, 13021.

(32) Margl, P.; Deng, L.; Ziegler, T. *J. Am. Chem. Soc.* **1999**, *121*, 154.
(33) Lohrenz, J. C. W.; Bühl, M.; Weber, M.; Thiel, W. *J. Organomet. Chem.* **1999**, *592*, 11.
(34) Petitjean, L.; Pattou, D.; Ruiz-Lopez, M.-F. *J. Mol. Struct. (THEOCHEM)* **2001**, *541*, 227.
(35) Vanka, K.; Chan, M. S. W.; Pye, C. C.; Ziegler, T. *Macromol. Symp.* **2001**, *173*, 163.
(36) Schellenberg, J.; Tomotsu, N. *Prog. Polym. Sci.* **2002**, *27*, 1925 and references reported therein.
(37) Ishihara, N.; Seimiya, T.; Kuramono, M.; Uoi, M. *Polym. Prepr. Jpn.* **1986**, *35*, 240.
(38) Minieri, G.; Corradini, P.; Zambelli, A.; Guerra, G.; Cavallo, L. *Macromolecules* **2001**, *34*, 2459.
(39) Minieri, G.; Corradini, P.; Guerra, G.; Zambelli, A.; Cavallo, L. *Macromolecules* **2001**, *34*, 5379.
(40) Yang, S. H.; Jo, W. H.; Noh, S. K. *J. Chem. Phys.* **2003**, *119*, 1824.
(41) Delly, B. *J. Chem. Phys.* **1991**, *94*, 7245.
(42) Press, W. H.; Flannery, B. P.; Teukolsky, S. A.; Vetterling, W. T. *Numerical Recipes, the Art of Scientific Computing*; Cambridge University Press: New York, 1986.
(43) Pulay, P. *J. Comput. Chem.* **1982**, *3*, 556.
(44) Csa'sza'r, P.; Pulay, P. *J. Mol. Struct.* **1984**, *114*, 31.
(45) Becke, A. D. *Phys. Rev. A* **1988**, *38*, 3098.
(46) Perdew, J. P.; Wang, Y. *Phys. Rev. B* **1992**, *45*, 13244.
(47) Perdew, J. P.; Chevary, J. A.; Vosko, S. H.; Jackson, K. A.; Pederson, M. R.; Singh, D. J.; Fiolhais, C. *Phys. Rev. B* **1992**, *46*, 6671.
(48) Tomotsu, N.; Ishihara, N.; Newman, T. H.; Malanga, M. T. *J. Mol. Catal. A* **1998**, *128*, 167.
(49) Eisch, J. J.; Caldwell, K. R.; Werner, S.; Krüger, C. *Organometallics* **1991**, *10*, 3417.
(50) Arlman, E. J.; Cossée, P. *J. Catal.* **1964**, *3*, 99.
(51) Kawamura-Kuribayashi, H.; Koga, N.; Morokuma, K. *J. Am. Chem. Soc.* **1992**, *114*, 8687.
(52) Yosida, T.; Koga, N.; Morokuma, K. *Organometallics* **1995**, *14*, 746.
(53) Ewen, J. A. *J. Am. Chem. Soc.* **1984**, *106*, 6355.
(54) Cavallo, L.; Guerra, G.; Oliva, L.; Vacatello, M.; Corradini, P. *Polym. Commun.* **1989**, *30*, 16.
(55) Longo, P.; Grassi, A.; Pellecchia, C.; Zambelli, A. *Macromolecules* **1987**, *20*, 1015.
(56) Ewen, J. A. *Proc. Int. Sym. Future Aspects of Olefin Polymerization*, Tokyo, 1986.
(57) Venditto, V.; Guerra, G.; Corradini, P.; Fusco, R. *Polymer* **1990**, *31*, 530.
(58) Furuyama, R.; Saito, J.; Ishii, S.; Mitani, M.; Matsui, S.; Tohi, Y.; Makio, H.; Matsukawa, N.; Tanaka, H.; Fujita, T. *J. Mol. Catal. A* **2003**, *200*, 31.
(59) Laverty, D. T.; Rooney, J. J. *J. Chem. Soc., Faraday Trans.* **1983**, *79*, 869.
(60) Brookhart, M.; Green, M. L. H. *J. Organomet. Chem.* **1983**, *250*, 395.
(61) Brookhart, M.; Green, M. L. H.; Wong, L. *Prog. Inorg. Chem.* **1988**, *36*, 1.

MA0497815